The quest for function in systems with two dynamic covalent bonds

Marić, Ivana

DOI:
10.33612/diss.167788912

6.

Tailorable Supramolecular-Based Hydrogels for Cell Culture

This chapter is part of a *submitted* patent application: I. Marić, S. Otto, C. G. Pappas. Tailor-Made Functionalized Self-Assembled Peptide (Nano)fibers and Hydrogels, and Methods and Uses Related Thereto.

This chapter is part of a *manuscript in preparation*: I. Marić, L. Yang, X. Li, G. M. Santiago, X. Qiu, C. G. Pappas, J. Dijksman, P. van Rijn, S. Otto. Tailorable Supramolecular-Based Hydrogels That Use Two Reversible Chemistries

6.1 Introduction

Currently, the field of material science relies on a strategy that involves understanding and mimicking structures and behaviors found in nature in order to develop materials that are potentially useful tools for different applications.[1] In particular, soft, synthetic biomaterials are being explored rapidly, as they may have suitable chemical and physical properties for application as extracellular matrices for tissue engineering.[2] Functional supramolecular polymers have been viewed as a powerful platform for such application, since they can be constructed from peptides[3] or peptide-amphiphiles,[4] containing binding sites for biologically functional ligands.[5] Cell adhesion motifs,[6] peptide sequences that can direct cell differentiation[7,] and susceptibility to degradation[8] are essential ingredients for successful three-dimensional cell growth within synthetic materials.[9] Responsiveness to stimuli, environmental adaptivity, and capacity to self-repair are also desired properties.[10,11] Above all, synthetic biomaterials are advantageous regarding batch-to-batch consistency in comparison to ill-defined, naturally occurring hydrogels, enabling the translation of basic research into clinical applications.[12,13]

The hydrogel discussed in **Chapter 5** is characterized by several properties that potentially make this system a tunable, bioactive scaffold that can stimulate cell fate processes. First, similarly to the ECM, the synthetic material possesses a fibrous structure, as it is prepared from one-dimensional assemblies of molecular stacking motifs. Through a previously established method for controlling the length of a supramolecular polymer[14] and by varying cross-linker density,[15] we hypothesize that mechanical properties of hydrogels can be systematically altered. Second, due to its peptide nature, the presented material has an excellent potential to be cytocompatible, as peptide-based hydrogels have proven high biocompatibility.[16] Third, building block **1** bears the NH-NH_2 group at the C-terminus of the peptide; this functionality facilitates hydrogelation through a mild and bioorthogonal acyl-hydrazone formation,[17] between a fiber-like supramolecular polymer and dialdehyde cross-linker (**Figure 6.1a**). The same reaction can allow attachment of carbonyl-functionalized biologically relevant ligands such as cells adhesion motifs (e.g., RGD, LDV)[6,18,19] or short peptide sequences known to direct differentiation of stem cells (e.g., laminin sequence IKVAV),[7,20] full-length proteins (e.g., vitronectin, a glycoprotein that promotes cell spreading)[21] and growth factors (insulin-like growth factor-1, IGF-1),[22] and peptide targets of matrix-metalloproteinases (MMPs)[8,23] which can degrade the material locally allowing migration of cell, while maintaining bulk gel stability (**Figure 6.1c-d**). Furthermore, it has been previously reported that hydrazine cross-linked hydrogels can exhibit covalently adaptable behavior, i.e., to mimic the stress relaxing ability of natural ECMs through reversible breaking and reforming of dynamic covalent cross-links.[24]

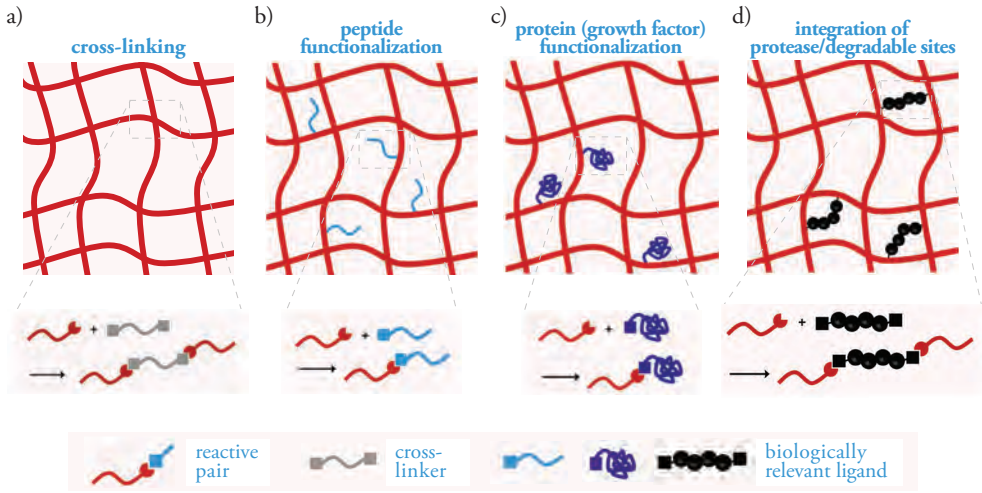

Figure 6.1 A synthetic strategy towards mimicking the native extracellular matrix. Acyl-hydrazone bond formation can be employed to achieve: **a)** cross-linking of peptide-based, fibrous self-assemblies yielding hydrogel formation; **b)** immobilization of bioactive short peptide sequences within the material; **c)** decoration of fibrillar scaffold with full-length proteins and growth factors, and **d)** tuning in protease-sensitive peptides as cross-linkers that would facilitate cell-induced enzymatic remodeling of the gel. As fibers bear NH-NH_2 groups, both cross-linkers and biologically relevant ligands need to be mono- or di- carbonyl-functionalized to form a reactive pair. This modular approach allows the molecular engineering of tailor-made material on demand.

In this chapter, we aim to evaluate the utility of the material developed in **Chapter 5** towards application in cell culturing. Previously described self-assembly driven supramolecular polymer $\mathbf{1}_5$ (**Chapter 3**; for the design of building block **1**, see **Section 3.2.1**; for the kinetic profile of formation of fiber-like structure $\mathbf{1}_5$ and its detailed characterization, see **Section 3.2.2**) was used as a fiber component for hydrogel formation. Using dynamic combinatorial chemistry,[14,25] self-assembly $\mathbf{1}_5$, can spontaneously emerge from a complex mixture of differently sized macrocycles made from **1**. The presence of the NH-NH_2 functionality at the C-terminus of building block **1**, i.e., at the surface of self-assembled fibers of $\mathbf{1}_5$, enables quick hydrogelation upon the addition of a di- or trialdehyde cross-linkers (**Chapter 5**). The same bond-forming reaction was exploited for the "decoration" of supramolecular assemblies by a small monoaldehyde, which were subsequently able to undergo hydrogelation due to cross-linking (**Chapter 5**, **Section 5.2.5**). This is of importance as we aim to develop a platform that can be decorated with carbonyl-functionalized biologically relevant ligands, to induce a specific cell response.

To gain a better insight into the material's composition, we determined the polydispersity index (PDI) values of the supramolecular polymers used for hydrogel formation.

Cytotoxicity assays suggest that human bone marrow-derived mesenchymal stem cells (hBM-MSCs) can proliferate without diminished viability in the presence of reported peptide-based material. Furthermore, cell adhesion-promoting sequences (**glyoxylyl-RGD** and **glyoxylyl-LDV**; **Scheme 6.1**) were incorporated into the hydrogel scaffold, and their influence on cell morphology was investigated. The *in vitro* results indicate strong binding and spreading of mesenchymal stem cells on the bioactive ligand-functionalized materials, but also on basic hydrogel matrix, based on compound **1**.

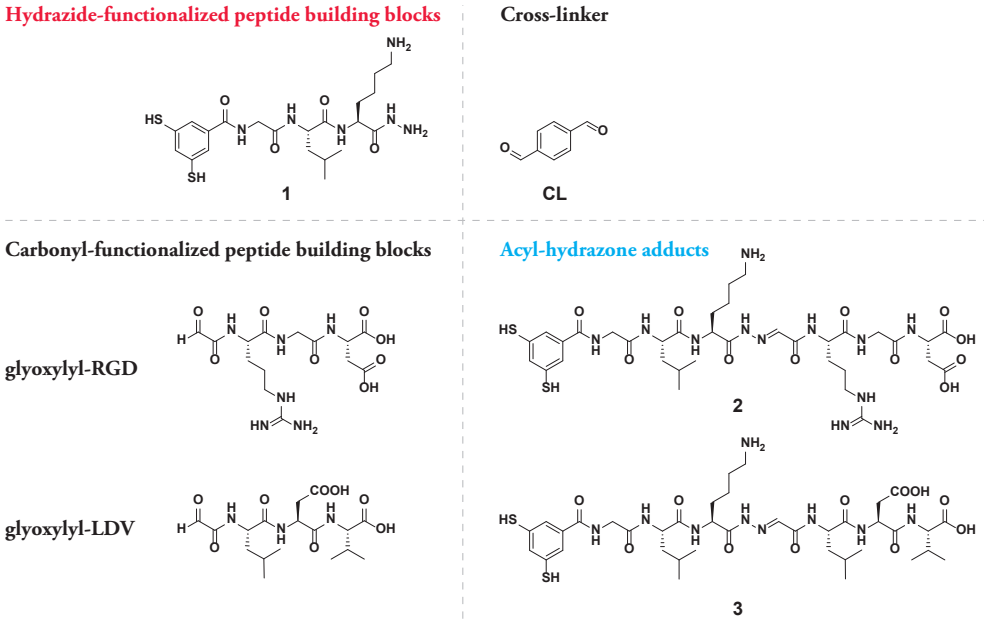

Scheme 6.1 Chemical structures of the hydrazide-functionalized peptide building block (**1**) used for the formation of fiber component ($\mathbf{1}_5$) of hydrogels; cross-linker (**CL**) terephthalaldehyde; carbonyl-functionalized, biologically-relevant peptide sequences (**glyoxylyl-RGD** and **glyoxylyl-LDV**), and acyl-hydrazone adducts formed upon addition of corresponding carbonyl-functionalized peptide building blocks to preformed $\mathbf{1}_5$ (adduct of **1** and **glyoxylyl-RGD** is denoted with **2**, **1** and **glyoxylyl-LDV** as **3**).

6.2 Results and Discussion

6.2.1 Determination of Polydispersity Index (PDI) of Self-Synthesizing Supramolecular Polymers

In general, incorporation of monomer units into a polymer chain through a polymerization reaction, results in a mixture of molecules that is not homogenous on a molecular level. Such heterogeneity is reflected in the various physical properties of a material; they

are not constant throughout the polymer sample.[26] To assess how much supramolecular uniformity varies between the batches of fiber components of hydrogels, which as a consequence, could influence the cell behavior, we set out to determine the polydispersity index (PDI) value.

As discussed in **Chapter 3, Section 3.2.2**, fiber growth is dependent on the agitation of the sample: input of mechanical energy induces fiber breakage, increasing the number of fiber ends from which the supramolecular polymer can grow. Although the growth of self-assembly $\mathbf{1}_5$ does not follow an exponential curve, we emphasize that mechanical agitation must play an essential role in $\mathbf{1}_5$ formation, as non-agitated samples remain dominated by non-assembled macrocycles (**Figure 6.2a**) after the same period. The outcome of stirred libraries are populations of fibers with a broad length distribution (**Figure S6.10**). The number-average length (L_n) of the library prepared following a general method and stirred at 1200 rpm was found to be 720 nm (**Figure 6.2b**). The PDI was 1.33 (**Figure 6.2c**), which is on the lower side compared to earlier reported examples of supramolecular polymers (PDI around 2),[27] but indicating that the samples are moderately polydisperse.

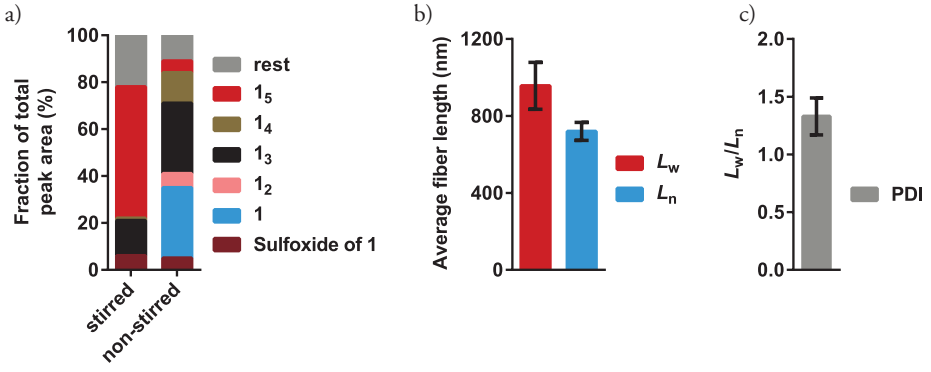

Figure 6.2 a) Effect of stirring on DCL composition made from building block **1** (4.0 mM) at 20°C after 20 days in borate buffer (12.5 mM, pH 8.2), stirred at 1200 rpm and without agitation; **b)** Weight-average (L_w) and number-average (L_n) fiber lengths of self-assemblies $\mathbf{1}_5$, obtained by oxidation and disulfide exchange of building block **1** (4.0 mM) in borate buffer (12.5 mM, pH 8.2) stirred at 1200 rpm; **c)** Consequent polydispersity index (PDI) of fibers $\mathbf{1}_5$. The plots **b)** and **c)** are based on 3 independent replicates.

6.2.2 Gel Stability in the Presence of Culture Media

Maintaining bulk stability and properties of the material on the time scale of cell culture experiments is essential, as the migration of cells to the stiff bottom of the culture container could lead to alteration of cell morphology. Such lack of stability would essentially reduce a 3D ECM model (if cells are encapsulated within the material) or 2D soft model (if cells are cultured on top of the soft material) to the traditional and static 2D culture on glass or plastic substrate. Both soft-material models are recognized as significantly more-true to tissue microenvironments[28] since stiffness can influence stem cell lineage specification,[29] morphology, and adhesion.[30]

Prior to encapsulating cells or seeding them on top of the gels, we tested compatibility between material and growth medium. The gels were prepared by a previously reported procedure (**Figure 6.3-i**), and a portion of the growth medium was added on top (**Figure 6.3-ii)**, to mimic the experiment involving cell seeding. The culture medium can diffuse inside the gel without any effect on the macroscopical level (**Figure 6.3-iii**), as evident by the red of the medium penetrating the gel, while the material remains undamaged. The gel is stable after prolonged incubation with culture medium (**Figure 6.3-vi**), indicating applicability in experiments that require long-term intactness of material.

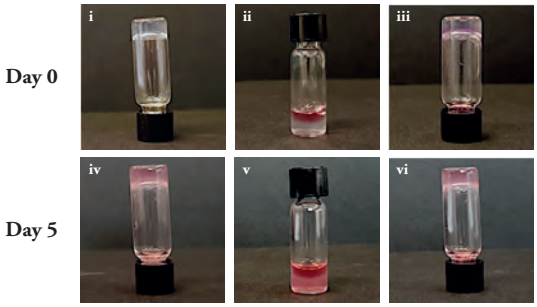

Figure 6.3 i) Gel formation (V = 300 μL, [**1**] = 4.0 mM) upon addition of terephthalaldehyde; **iv)** vial inversion test shows undamaged gel in presence of growth medium on day 5; **ii) and v)** addition of 200 μL of growth medium on gel (day 0 and day 5, respectively); **iii) and vi)** vial inversion test a few minutes after a new portion of the medium has been added (day 0 and day 5, respectively); before adding a new portion of the medium, the previous layer of the liquid has been removed. The gel exhibits stability for a couple of months.

6.2.3 Cytotoxicity Assessment of Hydrogels (Live/Dead and DAPI Staining)

The cytotoxic effect of the material was evaluated based on viability levels and proliferation rate of cells, as these parameters are good indicators of cell health. In general, cell viability and cytotoxicity assays are based on various cell functions, such as cell membrane integrity and permeability, enzyme activity, ATP production, etc.[31]

In order to quantify the survival of cells, live/dead analysis was performed using fluorescence microscopy. Human bone marrow-derived mesenchymal stem cells (hBM-MSCs) were seeded on top of the gels prepared by the previously established procedure, incubated for one day, and subsequently stained by two fluorescent dyes, calcein-AM and propidium iodide (PI) (for the protocol flowchart, see **Figure S6.1** and **Sections 6.5.6** and **6.5.7**). After a short-term culture, the material showed a minimal negative effect on cell viability, as there are more live cells (green dye) than dead cells (red dye) as shown in **Figure 6.4**. Quantification of the number of live cells per unit macroscopic field gave a mean of 91.0 ± 1.0%, among the three repetitions of the experiment.

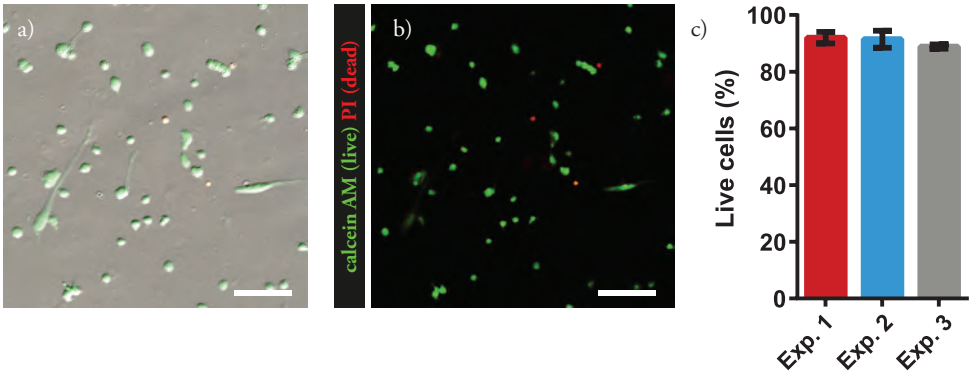

Figure 6.4 a) A representative transmitted light image and **b)** representative fluorescence microscopy image of human bone marrow-derived mesenchymal stem cells (hBM-MSCs) on hydrogel-coated glass coverslips in growth medium, stained with calcein-AM (live cells) and propidium iodide (dead cells), after 24 h. Scale bars equal to 150 μm. **c)** Quantification of cell viability cultured on hydrogel-coated glass coverslips in growth medium for three repetitions of the experiment. Mean ± SD (n=3, three random image fields per experiment).

To follow the change in cell number, staining with 4',6-diamidino-2-phenylindole (DAPI) at different time points, followed by fluorescence imaging was employed, as the dye strongly interacts with AT-rich regions of DNA within the nuclei (for the protocol,

see **Sections 6.5.6** and **6.5.8**). Visualization of cells within the population showed an increase in cell density over a period of five days (**Figure 6.5**), indicating that the material is suitable for cell survival and division. Furthermore, staining of the cytoskeleton with tetramethylrhodamine (TRITC)-phalloidin revealed that the cells do not show the rounded morphologies typical of apoptosis,[32] suggesting that the hydrogel chemistry is not intrinsically toxic.

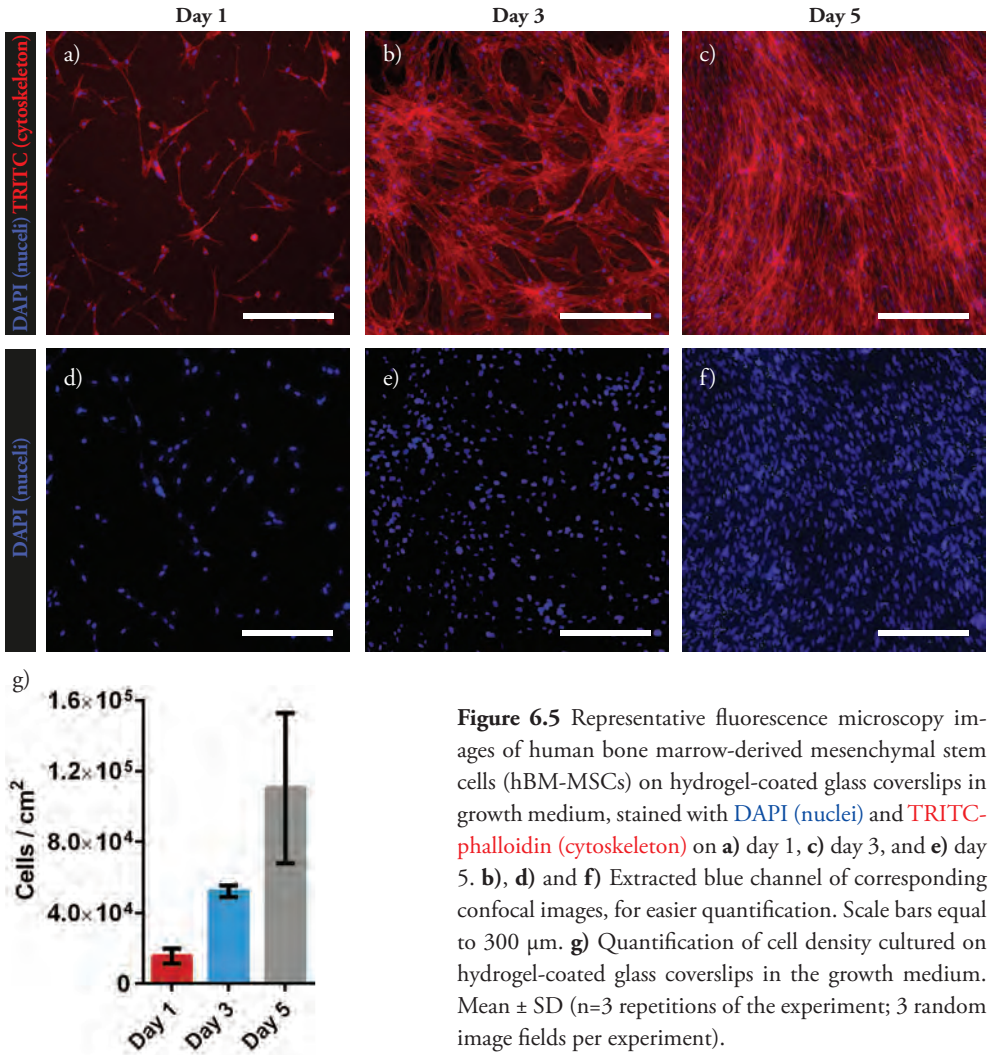

Figure 6.5 Representative fluorescence microscopy images of human bone marrow-derived mesenchymal stem cells (hBM-MSCs) on hydrogel-coated glass coverslips in growth medium, stained with DAPI (nuclei) and TRITC-phalloidin (cytoskeleton) on **a)** day 1, **c)** day 3, and **e)** day 5. **b)**, **d)** and **f)** Extracted blue channel of corresponding confocal images, for easier quantification. Scale bars equal to 300 μm. **g)** Quantification of cell density cultured on hydrogel-coated glass coverslips in the growth medium. Mean ± SD (n=3 repetitions of the experiment; 3 random image fields per experiment).

Overall, *in vitro* cytotoxicity tests (cell viability and cellular proliferation) indicate cytocompatibility of material based on building block **1** and cross-linker terephthalaldehyde (**CL**), which is the first step towards its application in tissue engineering.

6.2.4 Incorporation of Cell Adhesion Motives Into Fibrillar Scaffold

As discussed previously, the hydrogel based on building block **1** shows enough mechanical stability to support cells, as well as desired stability towards degradation by growth media, and is non-toxic. Another important remaining aspect is adequate interaction between the material and cells. Our approach focusses on the incorporation of biologically relevant ligands into the material, by post-assembly modification of peptide-based nanofibers and their subsequent hydrogelation. This "on-demand" chemically customized fibrillar scaffold potentially can promote a specific cell response.

6.2.4.1 Functionalization of Fibers with Cell Adhesion Signals and Their Hydrogelation

Supramolecular, self-assembled structure ($\mathbf{1}_5$) was obtained by oxidizing building block **1** under basic conditions ([**1**] = 4.0 mM) borate buffer (12.5 mM in $B_4O_7^{2-}$, pH 8.2). After UPLC/MS analysis confirmed that DCLs are dominated by $\mathbf{1}_5$ (**Figure 6.6a**), the preformed assembly was split into two and reacted with 10 mol% of **glyoxylyl-RGD** and **glyoxylyl-LDV**. Upon short-term stirring (30 min), UPLC traces of the two libraries showed partial covalent modification of $\mathbf{1}_5$ (**Figure 6.6b-c**). The reaction appears to be finished within 30 minutes, as a further change in library composition was not observed even upon prolonged stirring (20 h, **Figure S6.2,** and **Figure S6.5**). In general, incorporation of both carbonyl-functionalized peptide sequences led to the formation of mixed self-assemblies ($\mathbf{1}_4\mathbf{2}$, $\mathbf{1}_3\mathbf{2}_2$, and $\mathbf{1}_4\mathbf{3}$, $\mathbf{1}_3\mathbf{3}_2$, $\mathbf{1}_2\mathbf{3}_3$), while $\mathbf{1}_5$ also remained present. As remaining hydrazide groups ought to participate in hydrogel formation, partial covalent modification is desired. Atomic force micrographs of DCLs dominated by pentamer species functionalized with biologically relevant peptides demonstrate the presence of fibers (**Figure 6.6e-f**), similar to the original library composed of $\mathbf{1}_5$ (**Figure 6.6d**). Samples of post-modified fibers appear to be stable over a period of a couple of weeks, i.e., the composition of the library remains identical, although a slight loss of peak area was detected when samples were kept in the freezer between the measurements (**Figure S6.9**). The possibility for customized fibers to undergo hydrogelation upon the addition of terephthalaldehyde as a cross-linker was investigated. The concentration of remaining available hydrazide groups and the complemental functionalities of cross-linker (**CL**) was 1:1 and kept constant in hydrogelation experiments. Vial-inversion tests indicate gel formation in 2 minutes, for fibers both functionalized with **glyoxylyl-RGD** and **glyoxylyl-LDV** (**Figure 6.6g-h**).

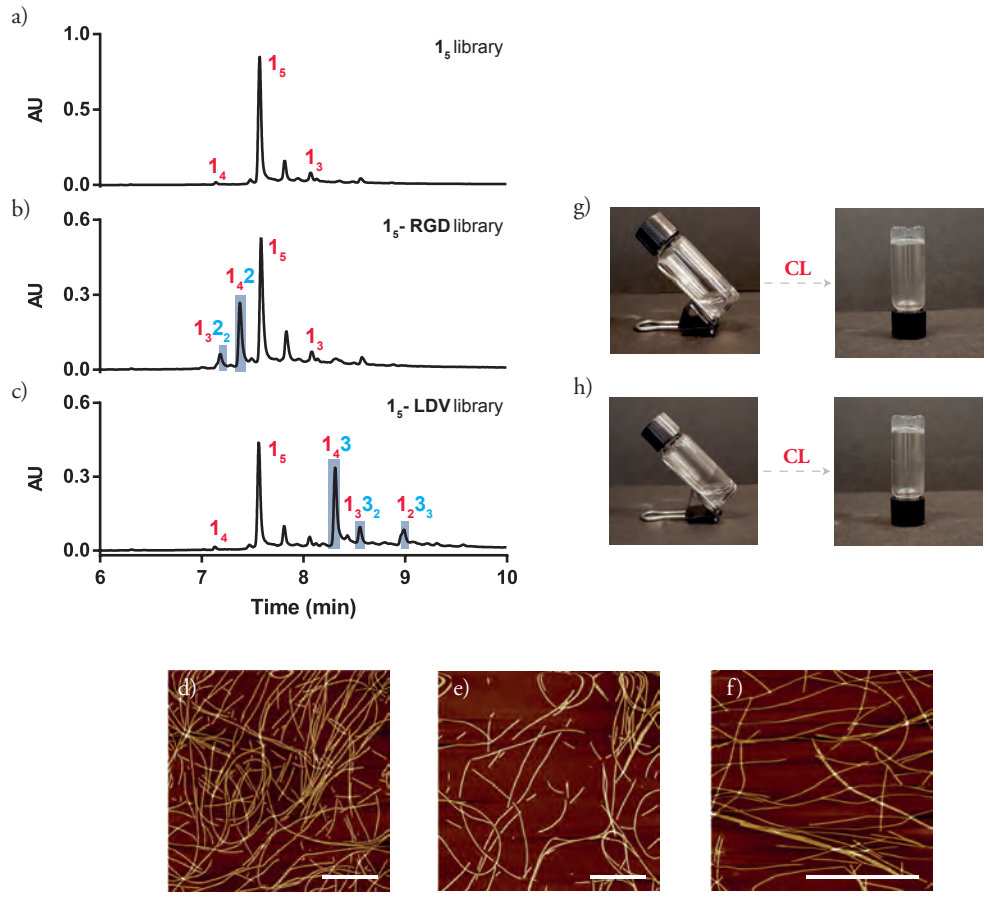

Figure 6.6 UPLC analyses of DCLs made by oxidation and disulfide exchange of **1** (4.0 mM) in borate buffer (12.5 mM, pH 8.2) stirred at 1200 rpm: **a)** when dominated by self-assembly $\mathbf{1}_5$; **b)** post-modification of $\mathbf{1}_5$ by **glyoxylyl-RGD ($\mathbf{1}_5$-RGD)** and **c) glyoxylyl-LDV ($\mathbf{1}_5$-LDV)**, both recorded 30 minutes after addition of the corresponding aldehydes. Formed acyl-hydrazones (mixed species) are highlighted in blue. Representative AFM images of DCLs **d)** dominated by $\mathbf{1}_5$; made by post-modification of $\mathbf{1}_5$ by **e) glyoxylyl-RGD** and **f) glyoxylyl-LDV**. Scale bars equal to 500 nm. Hydrogel formation upon addition of terphthalaldehyde (**CL**) to DCLs dominated by $\mathbf{1}_5$ and post-modified by **g) glyoxylyl-RGD ($\mathbf{1}_5$-RGD)** and **h) glyoxylyl-LDV ($\mathbf{1}_5$-LDV)**. The vial inversion test indicates the formation of hydrogels within 2 minutes after the addition of **CL**.

The above-discussed experiments show that acyl-hydrazone chemistry allows quick and efficient customization of nanofibers by biologically relevant ligands, as well as their hydrogelation. This approach can find application in the fabrication of versatile materials by simple "decoration" of the fibrillar scaffold.

6.2.5 Application of Tailored Gels in Cell Culture

Amino acid sequences RGD (R: arginine, G: glycine, D: aspartic acid)[18] and LDV (L: leucine, D: aspartic acid, V: valine)[19,33] are often employed peptides for stimulated cell adhesion on synthetic surfaces. RGD has been introduced into synthetic biopolymers formed by blending,[34] co-polymerization,[35] chemical[36] or physical treatment,[37] as stable covalent linking of the bioactive signal is a prerequisite for promoting cell spreading. The LDV motif has been applied for its cell adhesive properties, in chemical systems that can inhibit tumor metastasis[38] and soft materials for T-cell activation.[39]

Cell spreading and organization of actin cytoskeleton are events that characterize cell adhesion[40] and, therefore, are looked at when evaluating the effectiveness of materials functionalized with RGD or LDV. We performed live/dead staining of cells in the presence of material based on $\mathbf{1}_5$ and functionalized with **glyoxylyl-RGD** or **glyoxylyl-LDV**, to assess whether the presence of signaling peptides has an effect on cell viability. For identifying the influence of those peptide sequences on the morphology of the cells, hBM-MSCs were cultured on modified substrates and allowed to attach/spread for 1 day prior to visualization.

6.2.5.1 Live/Dead Viability Assay of Cells Cultured on Materials Containing Cell Adhesion Signals

Similar to the above-discussed evaluation of cytotoxicity of material based only on molecule **1**, the identical experiment was performed on cells cultured on substrates $\mathbf{1}_5$**-RGD** and $\mathbf{1}_5$**-LDV**. Following the previously established procedure, materials were prepared, cells were seeded and visualized upon incubation for one day (**Sections 6.5.3**, **6.5.6,** and **6.5.7**, respectively). The green (live) and red (dead) cells (**Figure 6.7a-c** and **Figure S6.11**) were manually counted in the three random domains per sample (n=3) per type of material. The results are shown in **Figure 6.7d**, which display the high viability of cells in all cases.

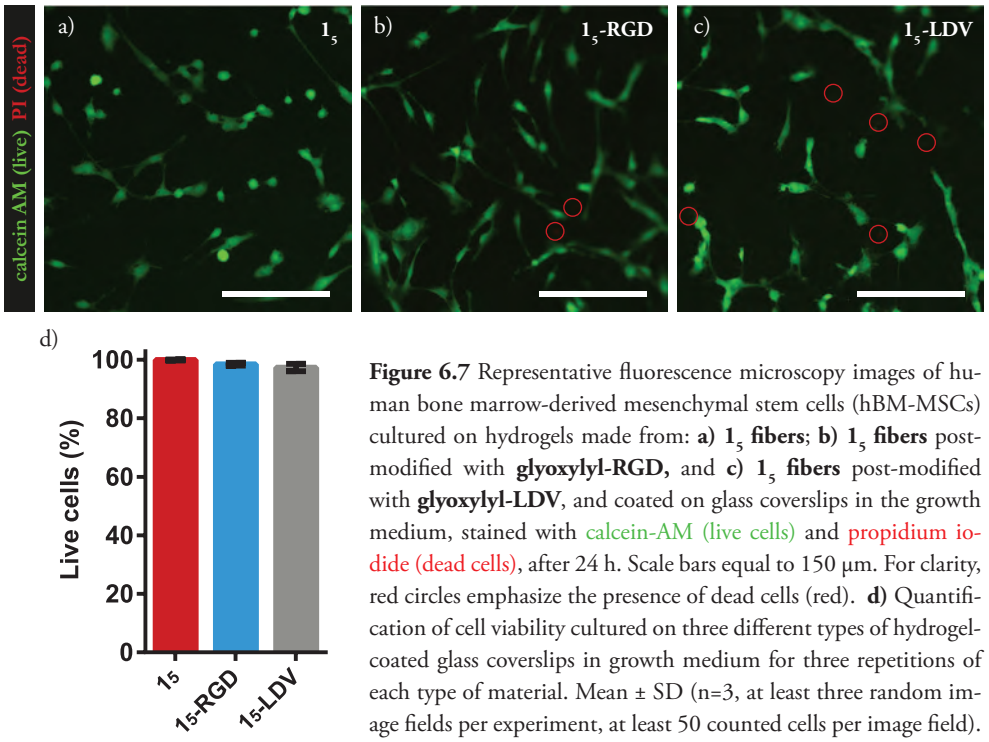

Figure 6.7 Representative fluorescence microscopy images of human bone marrow-derived mesenchymal stem cells (hBM-MSCs) cultured on hydrogels made from: **a) 1_5 fibers**; **b) 1_5 fibers** post-modified with **glyoxylyl-RGD,** and **c) 1_5 fibers** post-modified with **glyoxylyl-LDV**, and coated on glass coverslips in the growth medium, stained with calcein-AM (live cells) and propidium iodide (dead cells), after 24 h. Scale bars equal to 150 µm. For clarity, red circles emphasize the presence of dead cells (red). **d)** Quantification of cell viability cultured on three different types of hydrogel-coated glass coverslips in growth medium for three repetitions of each type of material. Mean ± SD (n=3, at least three random image fields per experiment, at least 50 counted cells per image field).

6.2.5.2 Influence of Material Type on Cell Morphology

To determine the effect of RGD and LDV sequence on the morphology of human bone marrow-derived mesenchymal stem cells, the cells were cultured on the original material based on **1_5** fibers and on substrates **1_5-RGD** and **1_5-LDV** for one day. After that, cells were fluorescently labelled to visualize their nuclei (DAPI) and cytoskeleton (FITC-phalloidin), (**Figure 6.8a-j**). From fluorescent imaging of the cytoskeleton (**Figures 6.8b, e, i**) it was observed that hBM-MSCs exhibit extended morphologies on all three types of materials, without significant discrepancies. The absence of notable effect of cell adhesion peptides on cell morphology, but also of cells with rounded morphology on the original substrate, indicate that peptide sequence of **1**, GLK, on its own promotes cell spreading. To the best of our knowledge, this peptide sequence has not been reported as a cell adhesion motif (naturally or synthetically derived) thus far.

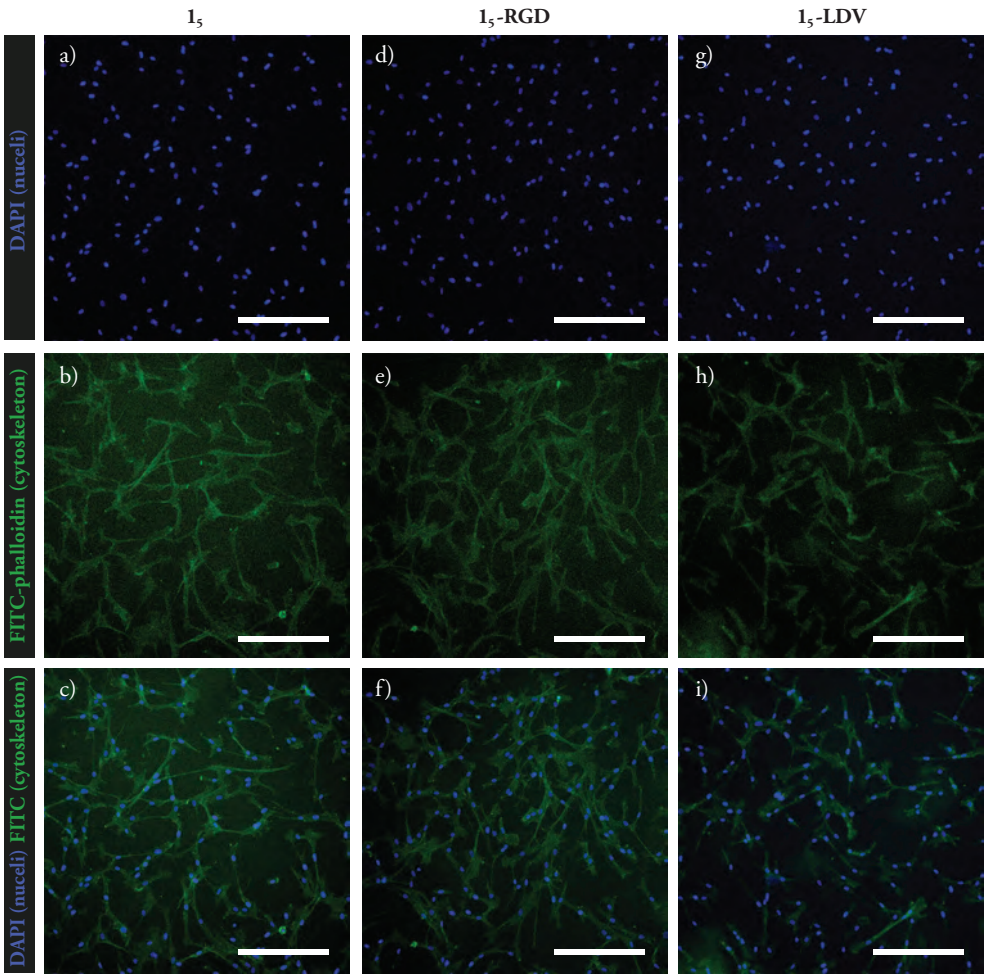

Figure 6.8 Representative fluorescence microscopy images of hBM-MSCs, cultured on hydrogels made from **a) – c)** **1_5 fibers**; **d) – f)** **1_5 fibers** post-modified with **glyoxylyl-RGD** and **g) – i)** **1_5 fibers** post-modified with **glyoxylyl-LDV**, stained with DAPI (blue) and FITC-phalloidin (cytoskeleton), after 24 h. The bottom images represent the merge of two channels. Scale bars equal to 300 μm.

6.3 Conclusions

The focus of the research discussed in this chapter was to investigate the applicability of material based on building block **1** as a synthetic alternative to the extracellular matrix. In summary, the presented fibrous network formed by cross-linking of products of peptide self-assembly showed to be biocompatible, as manifested in the high viability of cells when cultivated on presented hydrogels. In addition, upon prolonged cell cul-

ture, the number of hBM-MSCs significantly increased, indicating that the presented material does not interfere with any of the processes associated with the proliferation. After the first successful biological tests, we chemically "decorated" the fibrillar scaffold with peptide sequences isolated from proteins present in naturally-derived ECM, RGD, and LDV. As expected, incorporation of these cell adhesion motifs did not significantly alter (decrease) cytocompatibility of hydrogel materials. However, to our surprise, post-modified materials did not exhibit a notable influence on cell morphology compared to the material based solely on building block **1**. Visualization of cells revealed that cells in the original substrate's presence already display extended morphologies, characteristic for cell spreading and adhesion.

Since its identification as a minimal essential cell adhesion peptide sequence in fibronectin,[41] RGD has been incorporated into a large variety of synthetic materials. Very often, constituents of these materials have no resemblance with the building blocks found in nature (for example, PEG derivatives) but exhibit appropriate softness, and the presence of RGD is the single, chemical, point of contact with the ECM. Surprised by the extended morphologies grown on a substrate made of molecule **1**, which bears GLK sequence, we wondered: *Is the basic hydrogel matrix sufficiently cell-adhesive and its properties cannot be further improved?* or *Could it be that we identified a "new RGD"?* Hopefully, the ongoing research in our laboratories will soon answer these questions.

Regardless of this unexpected discovery, in this chapter, we established a methodology for the fabrication of tailor-made, molecularly engineered soft materials through a modular approach. The peptide-based nature of presented fibrous scaffolds makes them intrinsically biocompatible for cell culture. Other relevant peptide motifs have also been recognized,[42-44] which can potentially be immobilized onto functional materials. With the methodology in hand and as outlined in the Introduction of this chapter, we aim to tackle other versatile applications, while developing new matrices with combined biologically relevant ligands for more rigorous control over cell fate.

6.4 Acknowledgments

Dr. L. Yang is gratefully acknowledged for cell culture experiments, fluorescence, and confocal imaging. Dr. P. van Rijn and Dr. L. Yang are gratefully acknowledged for the discussion of results and generous help. Dr. M. Beatty is gratefully acknowledged for proof-reading this chapter and giving valuable feedback.

6.5 Materials and Methods

6.5.1 Materials

Boric anhydride (Sigma-Aldrich) and sodium hydroxide (Merck Chemicals) were utilized for buffer preparation and pH adjustments. The concentration of borate buffer is given in $B_4O_7^{2-}$ ions. Acetonitrile (UPLC-MS grade), water (UPLC-MS grade), DMF (HPLC grade), and trifluoroacetic acid (HPLC grade) were purchased from Biosolve BV. Building block **1** was purchased from Cambridge Peptides Ltd. (Birmingham, U.K.) and prepared by coupling 3,5-bis(tritylthio)benzoic acid, which was synthesized via a previously reported procedure[45] at the N-terminus. Terephthalaldehyde (**CL**) was purchased from TCI Chemicals. Glyoxylyl-RGD and glyoxylyl-LDV were purchased from Cambridge Peptides Ltd. (Birmingham, U.K.) and GenScript Biotech (Piscataway, New Jersey, USA), respectively. Gels were prepared on round, 12 mm diameter, and 0.17 mm thick borosilicate glass coverslips (Fischerbrand). Costar® multiple well plates (24 well, Corning® CellBIND® surface, polystyrene) were purchased from Corning and used for cell culture. Human bone marrow-derived mesenchymal stem cells (hBM-MSCs) were used for cell experiments. The growth medium supplemented with Alpha modified Eagle's medium (Gibco), 10% fetal bovine serum (Gibco), 0.1% ascorbic acid 2-phosphate (Sigma), and 1% penicillin/streptomycin (Gibco) and trypsin (Sigma-Aldrich) were utilized for cell culture and harvesting, respectively. Dyes propidium iodide and calcein-AM were obtained from Sigma-Aldrich and Thermo Fisher Scientific. For immunostaining cells were incubated with a primary antibody for vinculin (clone hVin-1, Sigma), followed by treatment with a secondary antibody Rhodamine Red™-X-labeled goat-anti-mouse antibody (Jackson Immunolab). The nucleus and cytoskeleton were stained with DAPI (4',6-diamidino-2-phenylindole) and FITC/TRITC-phalloidin purchased from Sigma-Aldrich. EM-grade PFA was purchased from Electron Microscopy Sciences.

6.5.2 Fiber Preparation and Sampling

Building block **1** was dissolved to a concentration of 4.0 mM in borate buffer (12.5 mM in $B_4O_7^{2-}$, pH 8.2). Due to **1** being a salt of TFA, the pH value had to be re-adjusted to 8.2 with 1 M NaOH. Subsequently, the solution was oxidized to approximately 40% with sodium perborate solution (40 mM). The sample was equilibrated in a UPLC vial (12 x 32 mm) with a Teflon-coated screw cap. The UPLC vial was equipped with a cylindrical

stirring bar (2 x 5 mm, Teflon-coated, purchased from VWR), and the solution was stirred at 1200 rpm using an IKA C-MAG HS 7 control hot plate stirrer. The temperature was kept constant at 25°C using a Thermo Scientific Compact Digital Dry Bath. The composition of the resulting DCL was monitored with UPLC. The progress of $\mathbf{1}_5$ formation was followed by sampling 5 μL of the DCL and diluting it to 50 μL with doubly distilled water. When DCL was dominated by $\mathbf{1}_5$, the sample was used directly since products of hydrazide hydrolysis were observed upon prolonged incubation.

6.5.3 Post-Modification of Fibers with Glyoxylyl-RGD and Glyoxylyl-LDV and Gel Preparation

Self-assembly $\mathbf{1}_5$ was obtained by oxidizing building block **1** under basic conditions ([**1**] = 4.0 mM, 12.5 mM borate buffer, pH 8.2). After UPLC/MS analysis confirmed that DCLs are dominated by assembly $\mathbf{1}_5$, 10 mol% of **glyoxylyl-RGD** and **glyoxylyl-LDV** were added, and libraries were stirred for another 30 min. The reaction between the aldehydes and $\mathbf{1}_5$ was confirmed by UPLC/MS, where mixed species ($\mathbf{1}_4\mathbf{2}/\mathbf{1}_3\mathbf{2}_2$ and $\mathbf{1}_4\mathbf{3}/\mathbf{1}_3\mathbf{3}_2$) were observed. To fiber solutions post-modified with peptide monoaldehydes, a portion of cross-linker **CL** was added to achieve hydrogelation. The remaining reactive groups of fibers and cross-linkers were kept constant at a molar ratio of 1:1.

6.5.4 Atomic Force Microscopy (AFM)

AFM samples were prepared by depositing 100 μL of a sample (diluted to 10 μM concentration in **1** with UPLC water) onto a clean mica surface (Grade V1, Van Loenen Instruments). Subsequently, the excess solvent was removed by blotting into a piece of paper, and the surface was washed twice with 100 μL UPLC grade water, blotted into a piece of paper, and finally dried in a gentle stream of air. The AFM measurements have been performed using a Bruker Multimode 8 instrument in ScanAsyst-Air imaging mode. Measurements were performed in air at room temperature. As a probe, a ScanAsyst Air (Bruker) silicon tip on a nitride cantilever was used with the following parameters: length: 115 μm, width: 25 μm, resonance frequency: 70 kHz, force constant: 0.4 N/m. The images were recorded with frequencies between 0.5 and 1.5 Hz and analyzed with NanoScope Analysis 1.50 software (Bruker Corporation, 2015). Analysis of the length distributions of the fibers was performed using ImageJ software. From different areas of the images, 100 fibers were selected, and a histogram was created by using bin and frequency function in Microsoft Excel. The average length and PDI were determined by calculating the number average fiber length (L_n) and weight average fiber

length (L_w) using equations 1-3. The latter was estimated from measurements of the contour lengths (L_i) of individual fiber, where N_i is the number of fibers of length L_i, and n is the number of fibers examined in each sample.

$$L_w = \frac{\sum_{i=1}^{n} N_i L_i^2}{\sum_{i=1}^{n} N_i L_i} \quad (1)$$

$$L_n = \frac{\sum_{i=1}^{n} N_i L_i}{\sum_{i=1}^{n} N_i} \quad (2)$$

The length distribution was characterized by the polydispersity index (PDI).

$$PDI = \frac{Lw}{Ln} \quad (3)$$

6.5.5 Cell Culture hBM-MSCs

Human bone marrow-derived mesenchymal stem cells (hBM-MSCs) from Lonza (passage 2) were cultured in a growth medium supplemented with Alpha modified Eagle's medium (Gibco), 10% fetal bovine serum (Gibco), 0.1% ascorbic acid 2-phosphate (Sigma), and 1% penicillin/streptomycin (Gibco). Cells were incubated at 37°C with 5% CO_2. Every 3 days, the culture medium was refreshed, and cells were passaged or harvested at approximately 80% confluence. The confluent cells were subcultured by trypsinization. hBM-MSCs of passage 4 were used for the next experiments.

6.5.6 Preparation of Gel-Coated Cover Slips and Cell Seeding

Glass coverslips were plasma treated for 5 min in PlasmaFlecto 10 to enhance the surface's wettability and adhesion. The reactive groups of fibers and cross-linkers were kept constant at a molar ratio of 1:1. The stock solution of cross-linker **CL** was prepared by dissolving the compound in acetone. Gels were prepared by mixing 100 µL of fiber solution (4.0 mM in building block **1**) with 2 µL of cross-linker stock solution, in an Eppendorf. Before gelation occurred, 25 µL (preliminary cytotoxicity experiments) or 50 µL (cytotoxicity of modified gels, cell morphology experiments) of the mixture was placed on top of the coverslip and left undisturbed until gelation was complete (app. 5 min). Coverslips were transferred into a 24-well plate. To each of the wells containing gel-coated coverslip, 250 µL of MiliQ water was added to prevent gel drying for the duration of UV-treatment. Gels were sterilized with UV-light for 15 minutes. After sterilization, cells were seeded on top of hydrogels at the app. 10000 cell/mL of culture medium (V = 1 mL per well), for all experiments. Plates were incubated at 37°C, 5%

CO_2, at maximum humidity. Live/dead staining was performed after 24 h, proliferation kinetics was followed for five days (day 1, 3, and 5), while cell morphology when cells are seeded on top or encapsulated was assessed after one day.

6.5.7 Live/Dead Staining

Live/dead staining was performed using propidium iodide and calcein-AM. Live cells were characterized by enzymatic conversion of cell-permeant, non-fluorescent calcein-AM into strongly fluorescent calcein (green) within live cells. Dead cells were characterized by propidium iodide as it binds to double-stranded DNA by intercalating between the bases but is excluded from cells with intact plasma membranes. Once the dye is bound, its fluorescence is enhanced 20- to 30-fold, producing a bright red fluorescence in dead cells. The working solution was prepared in serum-free media by adding propidium iodide (final concentration = 3 μM) and calcein-AM (final concentration = 5 μM) and protected from light. Culture media was removed, and hydrogels were washed with warm PBS, to which a sufficient amount of working solution to completely cover the sample (V = 400 μL) was added. Cells were incubated at 37°C for 20 minutes and subsequently visualized by fluorescence microscopy.

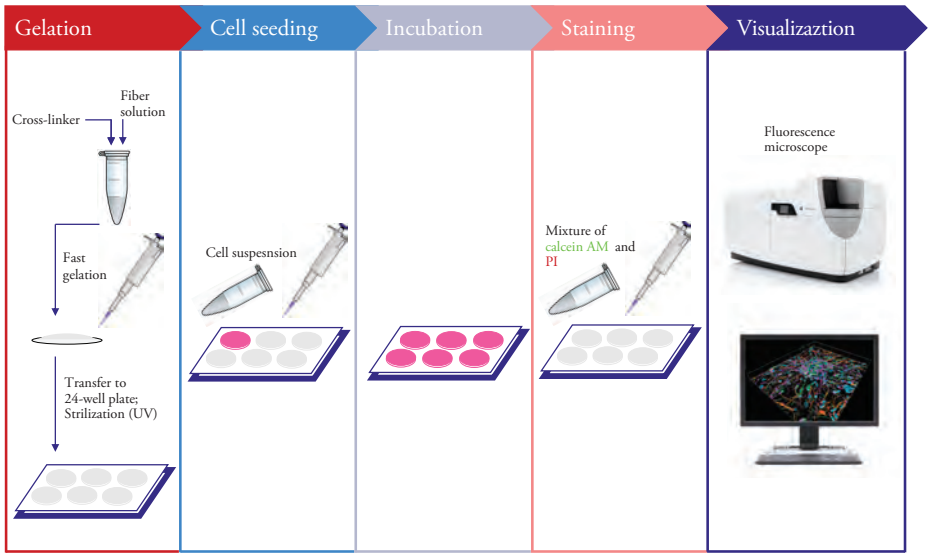

Figure S6.1 The protocol flowchart of preparation of gel-coated glass coverslips, cell seeding, live/dead staining, and visualization. Both sample preparation for proliferation kinetics and assessment of cell morphology were performed in a similar manner (for detailed procedures, see **Sections 6.5.8** and **6.5.9**, respectively).

6.5.8 Determination of Proliferation Kinetics by DAPI and TRITC-Labelled Phalloidin Staining

For the determination of proliferation kinetics, cells were rinsed with PBS and fixed for 15 min using warm 3.7% EM-grade paraformaldehyde (PFA) solution in PBS on days 1, 3, and 5. Afterward, the membrane of the cell was permeabilized with 0.5% Triton-X 100 solution in PBS for 3 min. The nucleus and cytoskeleton of fixed cells were visualized *in situ* with DAPI, a blue-fluorescent DNA stain that exhibits 20-fold enhancement of fluorescence upon binding to AT regions of dsDNA and TRITC-labelled phalloidin, that binds to actin filaments, respectively. The working solution was prepared in PBS containing 1% bovine serum albumin (BSA) by adding TRITC-labelled phalloidin (final concentration = 2 μg/mL) and DAPI (final concentration = 4 μg/mL) and protected from light. The hydrogels were incubated with a sufficient amount of working solution to completely cover the sample (V = 400 μL) in the dark, for an hour, and subsequently visualized by fluorescence microscopy.

6.5.9 Staining for Assessment of Cell Morphology

For assessment of cell morphology, cells were rinsed with PBS and fixed for 15 min using warm 3.7% EM-grade paraformaldehyde (PFA) solution in PBS after 24h. Afterward, the membranes of the cells were permeabilized with 0.5% Triton-X 100 solution in PBS for 3 min, and non-specific background was blocked with 5% bovine serum albumin (BSA) in PBS for 30 minutes. The nucleus and cytoskeleton of fixed cells were stained with DAPI and FITC-labelled phalloidin. The working solution was prepared in PBS containing 1% bovine serum albumin (BSA) by adding FITC-labelled phalloidin (final concentration = 2 μg/mL) and DAPI (final concentration = 4 μg/mL) and protected from light. The hydrogels were incubated with a sufficient amount of working solution to completely cover the sample (V = 400 μL) in the dark, for an hour, and subsequently visualized by fluorescence microscopy.

6.5.10 Encapsulation of Cells Inside the Gels

To assess the influence of different materials on cell morphology, we also wanted to culture the cells inside the hydrogels. Previously, it was observed that even a small amount of growth medium could prevent hydrogelation. To circumvent this issue, it is of importance to introduce the cells into the material with a minimum (ideally without) amount of residual growth medium. Thus, to encapsulate the cells, a solution of cells in growth medium was spun down to form a pallet of cells. The pallet was then separated from the growth medium and resuspended in an appropriate volume of fiber solution, to which a corresponding amount of cross-linker was added. As previously established (**Section 6.2.2**) addition of growth medium on top of the gels does not interfere with gel stability. Thus, the encapsulated cells in gels were layered with a portion of growth medium, providing the nutrients for cell survival. Nevertheless, staining and imaging of cells showed to be challenging. Following the established procedure for visualizations of nuclei and cytoskeleton did not lead to satisfying images that provide information about cell organization and/or morphology. The two dyes (DAPI and propidium iodide) non-selectively interacted with both material and cells, hampering accurate visualization of nuclei and cytoskeleton. Therefore, a new method for cell visualization is required.

6.5.11 Confocal Microscopy and Image Analysis

Cells were imaged with Celldiscoverer 7 with Plan-APOCHROMAT 5x/0.35 air objective (Carl Zeiss AG, Oberkochen, Germany) and TissueFaxs (TissueGnostics GmbH, Vienna, Austria) microscopes. Cell quantification was performed in ImageJ. Data are given as mean values ± standard deviation (SD).

6.6 UPLC and UPLC/MS Analyses

UPLC measurements were performed on a Waters Acquity UPLC H-class system equipped with a PDA detector. UPLC analyses were performed on an Acquity UPLC Peptide CSH C18 1.7 µm (150 x 2.1 mm) column, purchased from Waters, using UPLC-MS grade water (eluent **A**) and UPLC-MS grade acetonitrile (eluent **B**), containing 0.1 V/V % TFA as a modifier. A flow rate of 0.3 mL/min and a column temperature of 35°C were applied. Spectra were recorded at a detection wavelength of 254 nm.

UPLC-MS measurements were performed using a Waters Acquity UPLC H-class system coupled to Waters Xevo-G2 TOF. The mass spectrometer was operated in positive electrospray ionization mode with the following ionization parameters: capillary voltage: 3 kV, sampling cone voltage: 20 V, extraction cone voltage: 4 V, source gas temperature: 120°C, desolvation gas temperature: 450°C, cone gas flow (nitrogen): 1 L/h, desolvation gas flow (nitrogen): 800 L/h.

6.6.1 UPLC Method

t (min)	A (%)	B (%)
0.00	90.0	10.0
1.00	85.0	15.0
11.00	50.0	50.0
13.00	5.0	95.0
13.50	5.0	95.0
14.00	90.0	10.0
17.00	90.0	10.0

Table S6.1 UPLC method for the analysis of DCLs reported in **Chapter 6**.

6.6.2 UPLC and UPLC/MS Analysis of DCL Made From 1

The system based on building block **1** has already been reported in **Chapter 3**. For the detailed UPLC and UPLC/MS analysis, see **Section 3.8.2.1**.

6.6.3 UPLC and UPLC/MS Analysis of DCL Made From 1 and 2

Species	Elution Time (min)	
	UPLC	*UPLC/MS*
$\mathbf{1}_4$	7.03	7.59
$\mathbf{1}_3\mathbf{2}_2$	7.06	7.65
$\mathbf{1}_4\mathbf{2}$	7.25	7.83
$\mathbf{1}_5$	7.45	8.03
$\mathbf{1}_3$	8.05	8.59

Table S6.2 Elution times (in the UPLC and UPLC/MS chromatograms) of species formed by post-modification of $\mathbf{1}_5$ with **glyoxylyl-RGD**. Adduct of **1** and **glyoxylyl-RGD** is denoted with **2**. Mass spectra of species highlighted in blue are given in **Section 3.8.2.1**; therefore, their mass spectra are not shown again.

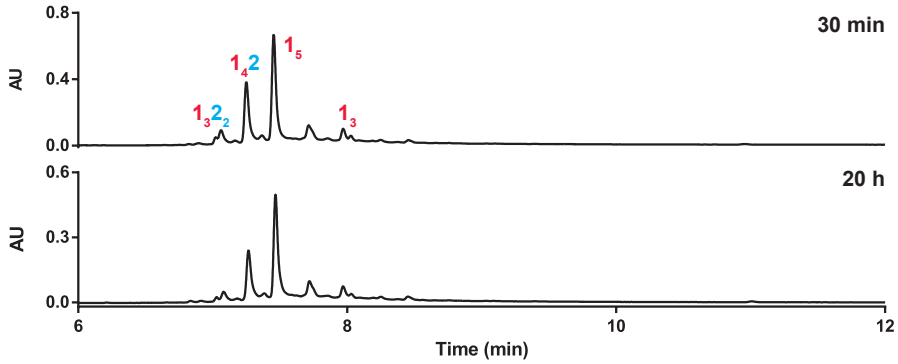

Figure S6.2 Relevant parts of the UPLC traces (monitored at 254 nm) of a DCL made by post-modification of preformed $\mathbf{1}_5$ (4.0 mM in building block **1**, 12.5 mM borate buffer, pH 8.2, stirred at 1200 rpm) by addition of **glyoxylyl-RGD**, at 30 min (**top**) and 20 h (**bottom**). Adduct of **1** and **glyoxylyl-RGD** is denoted with **2.**

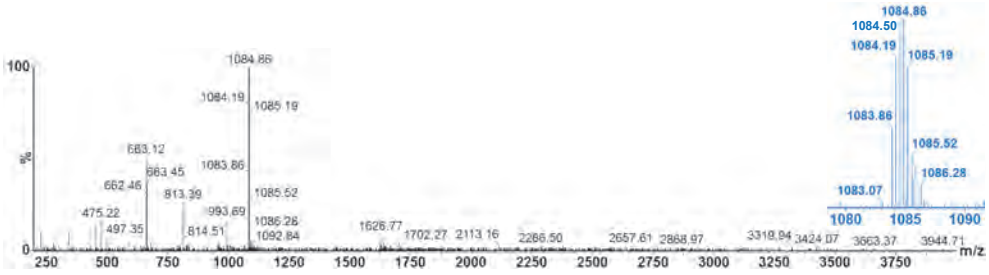

Figure S6.3 Mass spectrum of $\mathbf{1}_3\mathbf{2}_2$ (t_R = 7.65 min) from the LC-MS analysis of $\mathbf{1}_5$, post-modified with **glyoxylyl-RGD**. m/z calculated: 1626.66 $[M+2H]^{2+}$, 1085.11 $[M+3H]^{3+}$; m/z observed: 1626.77 $[M+2H]^{2+}$, 1083.86 $[M+3H]^{3+}$.

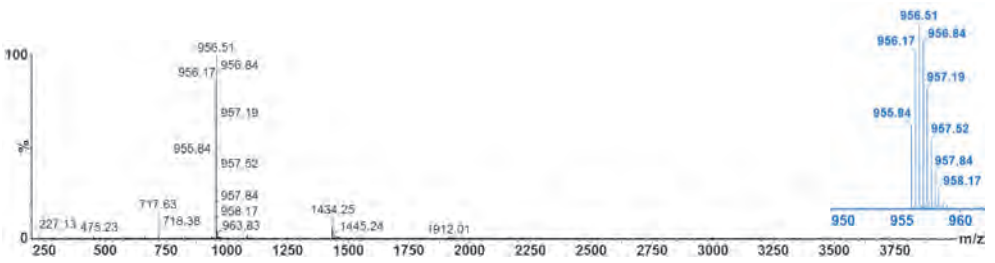

Figure S6.4 Mass spectrum of $\mathbf{1}_4\mathbf{2}$ (t_R = 7.83 min) from the LC-MS analysis of $\mathbf{1}_5$, post-modified with **glyoxylyl-RGD**. m/z calculated: 1434.59 $[M+2H]^{2+}$, 956.73 $[M+3H]^{3+}$; m/z observed: 1433.25 $[M+2H]^{2+}$, 955.84 $[M+3H]^{3+}$.

6.6.4 UPLC and UPLC/MS Analysis of DCL Made From 1 and 3

Species	Elution Time (min)	
	UPLC	*UPLC/MS*
$\mathbf{1}_4$	7.03	7.59
$\mathbf{1}_5$	7.47	8.03
$\mathbf{1}_3$	8.05	8.60
$\mathbf{1}_4\mathbf{3}$	8.22	8.78
$\mathbf{1}_3\mathbf{3}_2$	8.89	9.47
$\mathbf{1}_2\mathbf{3}_3$	9.48	10.05

Table S6.3 Elution times (in the UPLC and UPLC/MS chromatograms) of species formed by post-modification of $\mathbf{1}_5$ with **glyoxylyl-LDV**. Adduct of **1** and **glyoxylyl-LDV** is denoted with **3**. Mass spectra of species highlighted in blue are given in **Section 3.8.2.1**; therefore, their mass spectra are not shown again.

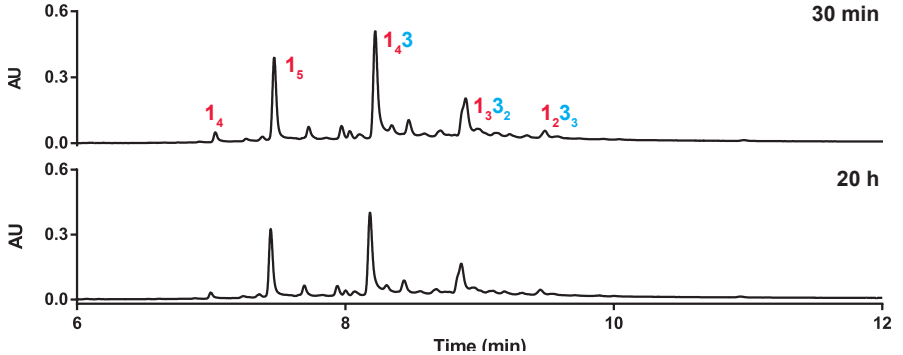

Figure S6.5 Relevant parts of the UPLC traces (monitored at 254 nm) of a DCL made by post-modification of preformed $\mathbf{1}_5$ (4.0 mM in building block **1**, 12.5 mM borate buffer, pH 8.2, stirred at 1200 rpm) by addition of **glyoxylyl-LDV**, at 30 min (**top**) and 20 h (**bottom**). Adduct of **1** and **glyoxylyl-LDV** is denoted with **3.**

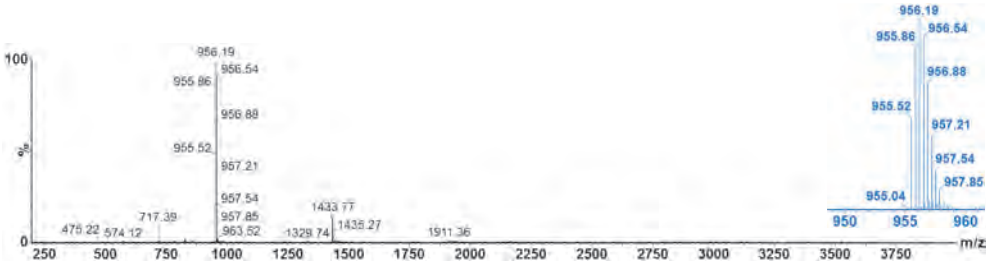

Figure S6.6 Mass spectrum of $\mathbf{1}_4\mathbf{3}$ (t_R = 8.78 min) from the LC-MS analysis of $\mathbf{1}_5$, post-modified with **glyoxylyl-LDV**. m/z calculated: 1434.11 $[M+2H]^{2+}$, 956.41 $[M+3H]^{3+}$, 717.55 $[M+4H]^{4+}$; m/z observed: 1432.78 $[M+2H]^{2+}$, 955.52 $[M+3H]^{3+}$, 716.89 $[M+4H]^{4+}$.

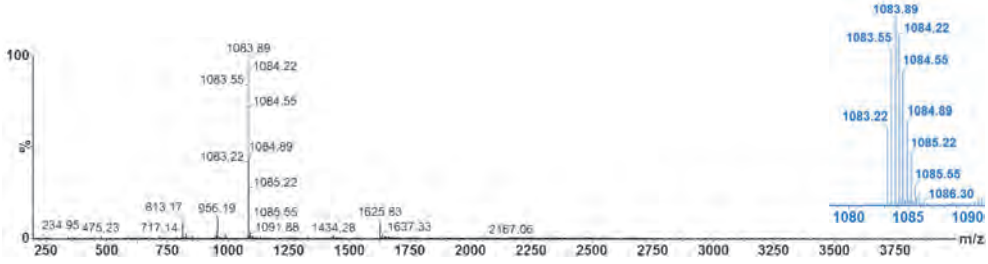

Figure S6.7 Mass spectrum of $\mathbf{1}_3\mathbf{3}_2$ (t_R = 9.47 min) from the LC-MS analysis of $\mathbf{1}_5$, post-modified with **glyoxylyl-LDV**. m/z calculated: 1625.69 $[M+2H]^{2+}$, 1084.46 $[M+3H]^{3+}$; m/z observed: 1624.33 $[M+2H]^{2+}$, 1083.22 $[M+3H]^{3+}$.

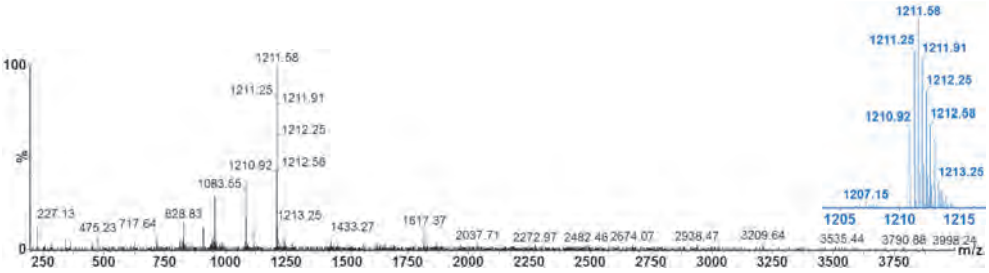

Figure S6.8 Mass spectrum of $\mathbf{1}_2\mathbf{3}_3$ (t_R = 10.05 min) from the LC-MS analysis of $\mathbf{1}_5$, post-modified with **glyoxylyl-LDV**. m/z calculated: 1817.28 $[M+2H]^{2+}$, 1212.19 $[M+3H]^{3+}$; m/z observed: 1816.37 $[M+2H]^{2+}$, 1210.92 $[M+3H]^{3+}$.

6.6.5 Stability of DCLs 1_5-RGD and 1_5-LDV Over Prolonged Period of Time

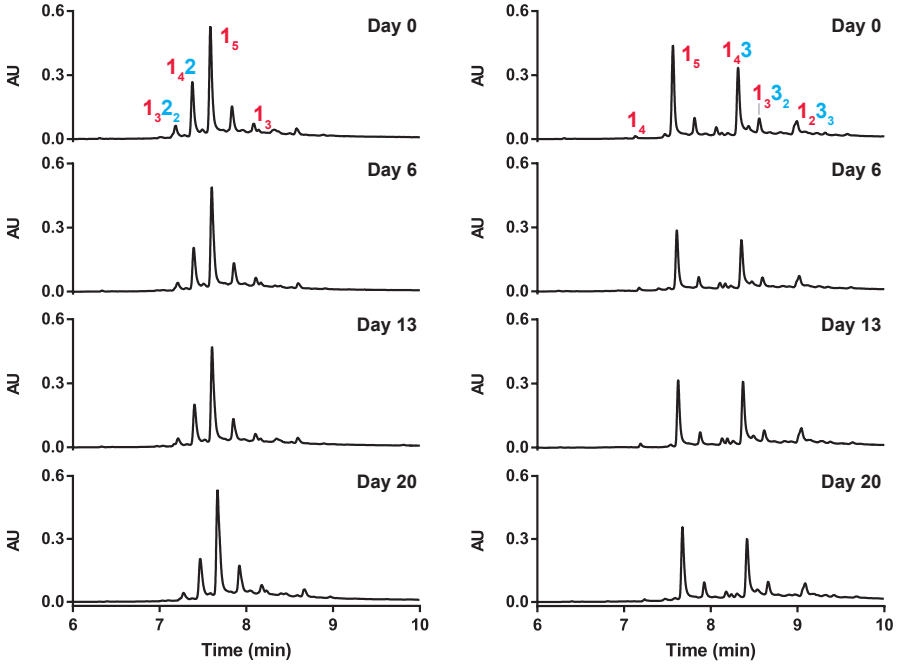

Figure S6.9 Relevant parts of the UPLC traces (monitored at 254 nm) of DCLs made by post-modification of preformed $\mathbf{1}_5$ (4.0 mM in building block **1**, 12.5 mM borate buffer, pH 8.2, stirred at 1200 rpm) by addition of **a) glyoxylyl-RGD** and **b) glyoxylyl-LDV** at different time points. The library compositions remain identical over a period of a couple of weeks when samples are stored in the freezer.

6.7 Histograms for Fiber Length Distribution

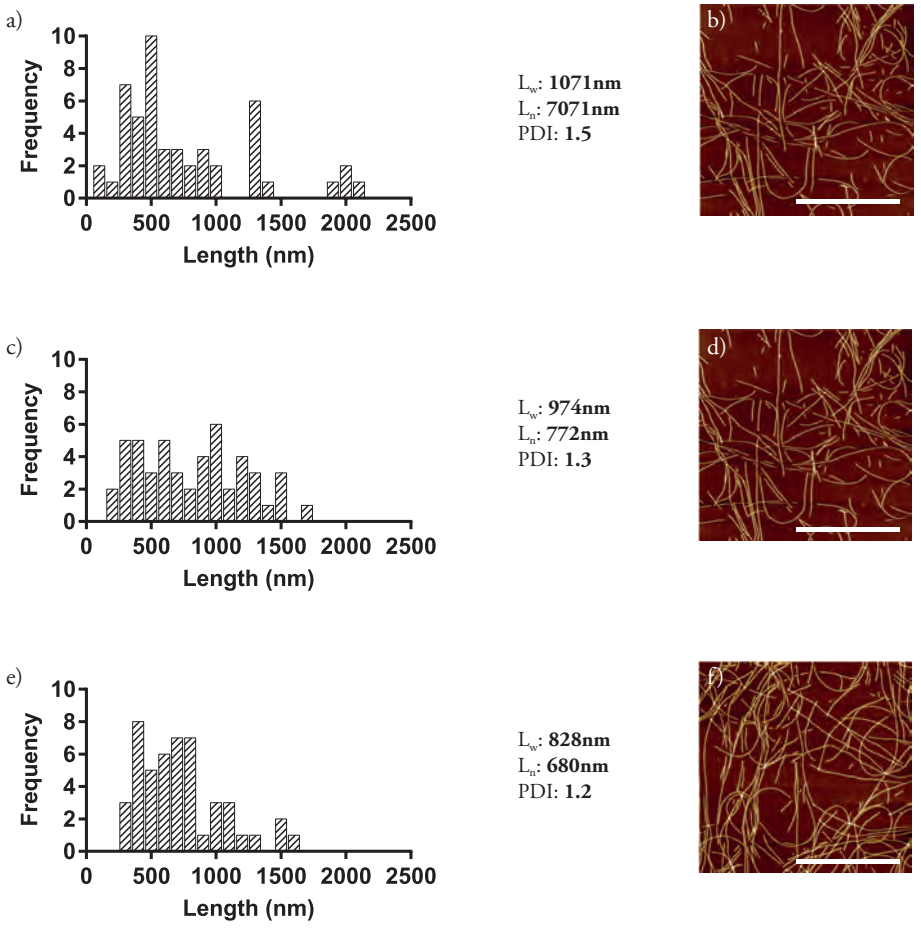

Figure S6.10 a), c) and **e)** Histograms for fiber length distribution and corresponding polydispersity indices of three independent DCLs dominated by self-assemblies $\mathbf{1}_5$, obtained by oxidation and disulfide exchange of building block **1** (4.0 mM) in borate buffer (12.5 mM, pH 8.2), stirred at 1200 rpm. **b), d)** and **f)** Representative AFM images of above mentioned DCLs. Scale bars equal to 1000 nm.

6.8 Supporting Images of Fluorescent Visualization of Cells

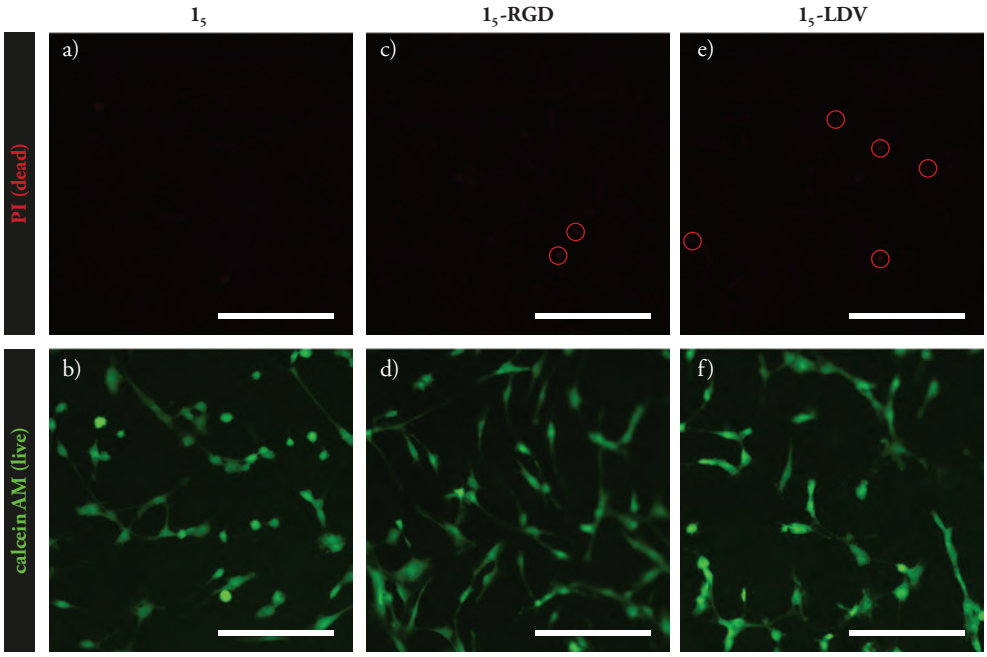

Figure S6.11 Representative fluorescence microscopy images of human bone marrow-derived mesenchymal stem cells (hBM-MSCs) cultured on hydrogels made from: **a), b) 1_5 fibers**; **c), d) 1_5 fibers** post-modified with **glyoxylyl-RGD** and **e), f) 1_5 fibers** post-modified with **glyoxylyl-LDV**, and coated on glass coverslips in the growth medium, stained with propidium iodide (dead cells) (top row, extracted channel) and calcein-AM (live cells) (bottom row, extracted channel), after 24 h. Scale bars are 150 μm. For clarity, red circles emphasize the presence of dead cells (red). The merge of red and green channels is given in **Figure 6.7**.

6.9 References

1 a) G. Jeronmidis, A. G. Atkins, J. *Mech. Eng. Sci.* **1995**, *209*, 221-235; b) P. Fratzl, *J. R. Soc. Interface* **2007**, *4*, 637-642; c) J. Aizenberg, P. Fratzl, *Adv. Mater.* **2009**, *21*, 387-388.

2 a) H. Shin, S. Jo, A. G. Mikos, *Biomaterials* **2003**, *24*, 4353-4364; b) P. X. Ma, *Adv. Drug. Deliv. Rev.* **2008**, *60*, 184-198; c) J. Patterson, M. M. Martino, J. A. Hubbell, *Mater. Today* **2010**, *13*, 14-22.

3 a) C. A. E. Hauser, S. Zhang, *Chem. Soc. Rev.*, **2010**, *39*, 2780-2790; b) S. Zhang, *Nat. Biotechnol.* **2003**, *21*, 1171-1178.

4 H. Cui, M. J. Webber, S. I. Stupp, *Biopolymers* **2010**, *94*, 1-18.

5 a) O. J. G. M. Goor, S. I. Hendrikse, P. W. Dankers, E. W. Meijer *Chem. Soc. Rev*. **2017**, *46*, 6621-6637; b) K. Sato, M. P. Hendricks, L. C. Palmer, S. I. Stupp, *Chem. Soc. Rev.* **2018**, *47*, 7539-7551.

6 P. Y. W. Dankers, M. C. Hamsen, L. A. Brouwer, M. J. A. van Luyn, E. W. Meijer, *Nat. Mater.* **2005**, *4*, 568-574.

7 G. A. Silva, C. Czeisler, K. L. Niece, E. Beniash, D. A. Harrington, J. A. Kessler, S. I. Stupp *Science*, **2004**, *303*, 1352-1355.

8 M. P. Lutolf, J. L. Lauer-Fields, H. G. Schmoekel, A. T. Metters, F. E. Weber, G. B. Fields, J. A Hubbel *Proc. Natl. Acad. Sci. USA*, **2013**, *100*, 9413-9418.

9 M. P. Lutolf, J. A. Hubbell, *Nat. Biotechnol.* **2005**, *1*, 47-55.

10 R. Yoshida, T. Okano in Biomedical *Applications of Hydrogels Handbook, Vol. XX* (Eds: R. M. Ottenbrite, K. Park, T. Okano), Springer-Verlag, New York, **2010**, pp. 19-43.

11 H. Wang, S. C. Heilshorn, *Adv. Mater.* **2015**, *27*, 3717-3736.

12 P. Worthington, J. Pochan, S. A. Langhans, *Front. Oncol.* **2015**, *92*, 1-10.

13 D. Seliktar, *Science* **2012**, *336*, 1124-1128.

14 A. Pal, M. Malakoutikhah, G. Leonetti, M. Tezcan, M. Colomb-Delsuc, V. D. Nguyen, J. van der Gucht, S. Otto, *Angew. Chem. Int. Ed.* **2015**, *54*, 7852-7856.

15 V. D. Nguyen, A. Pal, F. Snijkers, M. Colomb-Delsuc, G. Leonetti, S. Otto, J. van der Gucht, *Soft Matter* **2016**, *12*, 432-440.

16 a) A. N. Jonker, D. W. P. M. Löwik, J. C. M. van Hest, *Chem. Mater.* **2012**, *24*, 759-773; b) J. Li, R. Xing, S. Bai, X. Yan, *Soft Matter.* **2019**, *15*, 1704-1715.

17 J. Kalia, R. T. Raines, *Curr. Org. Chem.* **2010**, *14*, 138-147.

18 U. Hersel, C. Dahmen, H. Kessler, *Biomaterials*, **2003**, *24*, 4395-4415.

19 M. C. Cringoli, C. Romano, E. Parisi, L. J. Waddington, M. Melchionna, S. Semeraro, R. De Zorzi, M. Grönholm, S, Marchesan, *Chem. Commun.* **2020**, *56*, 3015-3018.

20 R. Patel, M. Santosh, J. Kumar Dash, R. Karpoormath, A. Jha, J. Kwak, M. Patel, J. Hak Kim, *Polym. Adv. Technol.* **2018**, *30*, 1-9.

21 E. G. Hayman, M. D. Pierschbacher, Y. Ohgren, E. Ruoslahti, *Proc. Natl. Acad. Sci. USA* **1983**, *80*, 4003-4007.

22 a) G. Feng, J. Zhang, Y. Li, Y. Nie, D. Zhu, R. Wang, J. Liu, J. Gao, N. Liu, N. He, W. Du, H. Tao, Y. Che, Y. Xu, D. Kong, Q. Zhao, Z. Li, *J. Am. Soc. Nephrol.* **2016**, *27*, 2357-2369; b) A. K. A. Silva, C. Richard, M. Bessodes, D. Scherman, O.-W. Merten, *Biomacromolecules*, **2009**, *10*, 9-18; c) Z. Li, Y. Xu, H. Li, *Sci. China.*

Chem. **2014**, *57*, 568-578.

23 a) J. Patterson, J. A. Hubbell, *Biomaterials*, **2010**, *30*, 7836-7845; b) Y. Shi, D. S. Ferreira, J. Banerjee, A. R. Pickford, H. S. Azevedo, *Biomater. Sci.* **2019**, *7*, 5132-5142; c) J. Son, D. Kalafatovic, M. Kumar, B. Yoo, M. A. Cornejo, M. Contel. R. V. Ulijn, *ACS Nano*, **2019**, *13*, 1555-1562.

24 D. D. McKinnon, D. W. Domaille, J. N. Cha, K. S. Anseth, *Adv. Mater.* **2014**, *26*, 865-872.

25 a) M. Malakoutikhah, M. Colomb-Delsuc, H. Fanlo-Virgós, J. J.-P. Peyralans, M. C. A. Stuart, S. Otto, *J. Am. Chem. Soc*. **2013**, *135*, 18406-18417; b) P. Nowak, M. Colomb-Delsuc, S. Otto, J. Li*, J. Am. Chem. Soc*. **2015**, *137*, 10965-10969.

26 M. Rogošić, H. J. Mencer, Z. Gomzi, *Eur. Polym. J.* **1996**, *11*, 1337-1344.

27 T. F. A. De Greef, M. M. Smulders, M. Wolffs, A. P. Schenning, R. P. Sijbesma, E. W. Meijer, *Chem. Rev.* **2009**, *109*, 5687-5754

28 B. M. Baker, C. S. Chen, *J. Cell Sci.* **2012**, *125*, 3015-3024.

29 A. J. Engler, S. Sen, H. L. Sweeney, D. E. Discher, *Cell*, **2006**, *126*, 677-689.

30 M. Sun, G. Chi, P. Li, S. Lv, J. Xu, Z. Xu, Y. Xia, Y. Tan, J. Xu, L. Li, Y. Li, *Int. J. Med. Sci.* **2018**, *15*, 257-268.

31 Ö. S. Aslantürk, *In Vitro Cytotoxicity and Cell Viability Assays: Principles, Advantages, and Disadvantages* in *Genotoxicity - A Predictable Risk to Our Actual World (Eds.: M. L. Larramendy, Sonia Soloneski)* IntechOpen, **2017**, pp 1-17.

32 G. Häcker, *Cell Tissue Res.* **2000**, 301, 5-17.

33 R. De Marco, A. Greco, N. Calonghi, S. D. Dattoli, M. Baiula, S. Spampinato, P. Picchetti, L. De Cola, M. Anslemi, F. Cipriani, L. Gentilucci, *Biopolymers*, **2017**, e23081.

34 A. W. Morgan, K. E. Roskov, S. Lin-Gibson, D. L. Kaplan, M. L. Becker, C. G. Simon Jr. *Biomaterials*, **2008**, *29*, 2556-2563.

35 D. A. Barrera, E. Zylstra, P. T. Lansbury, R. Langer, *J. Am. Chem. Soc.* **1993**, *115*, 11010-11011.

36 K. Kugo, M. Okuno, K. Masuda, J. Nishino, H. Masuda, M. Iwatsuki, *J. Biomater. Sci. Polym. Ed.* **1998**, *9*, 629-652.

37 E. S. Carlisle, M. R. Mariappan, K. D. Nelson, B. E. Thomas, R. B. Timmons, A. Constantinescu, R. C. Eberhart, P. E. Bankey, *Tissue Eng.* **2000**, *6*, 45-52.

38 Y. Kaneda, Y. Yamamoto, N. Okada, Y. Tsutsumi, S. Nakagawa, M. Kakiuch, M. Maeda, K. Kawasaki, T. Mayumi, *Anti-Cancer Drugs*, **1997**, *8*, 702-707.

39 J. Guasch, C. A. Muth, J. Diemer, H. Riahinezhad, J. P. Spatz, *Nano. Lett.* **2017**, *17*, 6110-6116.

40 R. G. Lebaron, K. A. Athanasiou, *Tissue Eng.* **2000**, *6*, 95-103.

41 M. D. Pierschbacher, E. Ruoslahti, *Nature*, **1984**, *309*, 30-33.

42 P. Ung, D. A. Winkler, *J. Med. Chem.* **2011**, *54*, 1111-1125.

43 K. Shiba, *Chem. Soc. Rev.* **2010**, *39*, 117-126

44 S. Caputi, O. Trubiani, B. Sinjari, S. Trofimova, F. Diomed, N. Linkova, A. Diatlova, V. Khavinson, *Int. J. Immunopath. Ph.* **2019**, *33*, 1-12.

45 J. M. A. Carnall, C. A. Waudby, A. M. Belenguer, M. C. A. Stuart, J. J.-P. Peyralans, S. Otto, *Science*, **2010**, *327*, 1502-1506.